The CathPilot: Performance Validation and Preclinical Safety and Feasibility Assessment

James J. Zhou, Yara Alawneh, Alykhan Sewani, Mohammadmahdi Keshavarz,
Mohammadmahdi Tahmasebi, Trisha Roy, Ahmed Kayssi, Andrew Dueck, Graham A. Wright,
and M. Ali Tavallaei

Abstract—*Objectives*: **Peripheral endovascular revascularization procedures often fail due to technical limitations of guidewire support, steering, and visualization. The novel CathPilot catheter aims to address these challenges. This study assesses the safety and feasibility of the CathPilot and compares its performance to conventional catheters for peripheral vascular interventions. *Methods*: The study compared the CathPilot to non-steerable and steerable catheters. The success rates and access times for a relevant target inside a tortuous vessel phantom model were assessed. The reachable workspace within the vessel and the guidewire's force delivery capabilities were also evaluated. To validate the technology, chronic total occlusion tissue samples were used ex vivo to compare crossing success rates with conventional catheters. Finally, in vivo experiments in a porcine aorta were conducted to evaluate safety and feasibility. *Results*: The success rates for reaching the set targets were 31%, 69%, and 100% with the non-steerable catheter, the steerable catheter, and the CathPilot, respectively. CathPilot had a significantly larger reachable workspace, and allowed for up to four times higher force delivery and pushability. In crossing of chronic total occlusion samples, the CathPilot achieved a success rate of 83% and 100%, for fresh and fixed lesions respectively, which was also significantly higher than conventional catheters. The device was fully functional in the in vivo study, and there were no signs of coagulation or damage to the vessel wall. *Conclusion*: This study shows the safety and feasibility of the CathPilot system and its potential to reduce failure and complication rates in peripheral vascular interventions. The novel catheter outperformed conventional catheters in all defined metrics. This technology can potentially improve the success rate and outcome of peripheral endovascular revascularization procedures.**

Index Terms—**Peripheral vascular interventions, angioplasty, atherectomy, non-steerable catheter, steerable catheter, catheter navigation, catheter manipulation, catheter limitations, peripheral artery disease, chronic total occlusions, guidewires, endovascular, CathPilot.**

I. INTRODUCTION

PERIPHERAL artery disease (PAD) affects more than 12% of adults. In this disease, the narrowing of the blood vessels restricts the flow of blood to the lower extremities [1]. Patients with PAD may develop intermittent claudication, limiting their quality of life [2]. Without revascularization, PAD can progress to critical limb ischemia (CLI), with associated chronic pain, non-healing sores, and gangrene which results in a 40% amputation rate within the first year of diagnosis [3], [4] and an overall 20-25% mortality rate [5].

PAD is typically treated with minimally invasive peripheral vascular interventions, either with plaque removal or angioplasty. The success of these procedures hinges on the guidewire's ability to successfully traverse the plaque. Utilizing x-ray fluoroscopy, clinicians navigate a guidewire and catheter to the site of the stenosis or occlusion; then, they advance the guidewire through the plaque, establishing a pathway for subsequent revascularization devices to effectively treat the affected vessel [1].

Unfortunately, with conventional tools, endovascular revascularization suffers from significantly high failure rates (15-20%) [6] and complication rates [7], [8]. Generally, these failures are immediate technical failures primarily due to the inability of the guidewire to cross the lesion[6]. This failure is despite the highly frequent presence of microchannels as well as softer penetrable segments within peripheral chronic total occlusions (CTOs), which are known to be extremely heterogeneous [9], [10], [11], [12]. Effectively accessing and penetrating these sections of plaque require accurate navigation and support of the corresponding interventional devices used in these procedures.

Like other catheter-based procedures, peripheral revascularization depends on conventional catheters that are long, flexible, and passive devices requiring manual manipulation from outside the patient body [13], [14]. We believe the root cause of the current high failure rates for endovascular revascularization are limitations of conventional catheters and guidewires in terms of guidewire support and its steering and navigation relative to the artery and plaque. There are three key factors to these limitations.

First, the patient's anatomy mechanically impacts the position of the guidewire and/or catheter, as the devices are highly flexible and engage with the vessel wall along their full length. Second, x-ray fluoroscopy does not provide 3D anatomical information and depth perception needed to facilitate accurate tip placement in a volume. Third, the long and flexible guidewires buckle under pressure as they engage the occlusion and attempt to penetrate it. These challenges to device support and navigation contribute to longer procedure times, extended radiation exposure, and a high failure and complication rates [15].

To understand this problem, in a previous study, we quantified the performance of a non-steerable catheter (N-SC) and steerable catheter (SC) in the context of a tortuous endovascular revascularization phantom, in which we compared the reachable workspace, the force delivery, and the success rates in crossing 3D printed and ex vivo lesions [15]. The N-SC and SC could only effectively reach 45% and 68% of the artery cross-section, respectively. In benchtop phantom experiments, this steering limitation manifested as high failure rates for crossing 3D-printed lesions. In addition, neither catheter could support the device sufficiently to permit the delivery of expected forces for penetration of such heterogeneous lesions [15]. Finally, with the N-SC, users could only cross 9.5% of freshly excised CTOs ex vivo successfully. This research confirmed the need to directly address the limitations of conventional tools and catheters used in the endovascular treatment of PAD.

In an attempt to address some of these limitations, engineers have developed electro-mechanical catheter navigation platforms that robotically operate tendon-based steerable catheters. These platforms keep the surgeon in a safe and ergonomic setting away from the ionizing radiation source [16]. However, this technology still relies on a conventional steering catheter; any steering inputs still contend with the mechanical interactions between the anatomy and the device. Thus, these systems do not *directly* address the limitations of catheter-based procedures.

Electromagnetic catheter navigation systems, on the other hand, directly address the problem with catheter steering; a commercially available example is the Stereotaxis Niobe [17]. They allow for direct manipulation of the catheter tip using electromagnetic gradients. The steering is, therefore, independent of the mechanical engagements between the catheter shaft and the anatomy. However, these systems are cost-prohibitive; they require expensive custom devices, a magnetic field source, and a dedicated catheterization lab. They also manipulate and track the device relative to a ground coordinate system and not the anatomy [14], [18] which is what the surgeon is primarily concerned with.

To address the visualization problem, there are technologies that implement electromagnetic-based tracking and fibre optic sensing (e.g., Fibre Bragg Grating) [19], [20]. They can provide improved 3D position and orientation information over conventional x-ray fluoroscopy. However, one limitation of such technologies is that they require expensive custom devices with integrated sensors. Such systems also report tracking relative to a defined reference coordinate system instead of the anatomy, the prime concern for the physician. Such systems also only address the visualization challenge. Visualizing the device and

target does not necessarily overcome the difficulties of steering, pushability, and navigation to reach the target.

To efficiently address the described challenges in steering, pushability, and visualization, a new steerable catheter—called the CathPilot—was recently developed [21]. We hypothesize that the CathPilot can outperform conventional catheters within the context of endovascular peripheral artery revascularization and that it is safe and feasible for use in vivo. Therefore, the main contributions of this article are as follows:

- Quantifying the performance of the CathPilot in terms of reachable workspace (i.e., navigation and steerability) and deliverable forces (i.e., pushability) and comparison to conventional catheters.
- Comparing the performance of the CathPilot with conventional catheters in crossing of actual CTO samples obtained from patients suffering from CLI and with failed endovascular revascularization attempts.
- Demonstrating system feasibility and safety in vivo within animal models.

II. METHODS

To quantitatively characterize and compare the performance of the CathPilot with conventional catheters (i.e., N-SC and SC catheters) within the context of applications for peripheral revascularization, we utilized the findings and the experimental protocols developed by Alawneh et al. [15], which characterized and compared conventional N-SC (GLIDECATH 4Fr, Terumois, Tokyo, Japan) with a SC (Agilis^{TM} NxT 8.5 Fr, Abbott Laboratories, Chicago, IL, USA). The experiments presented in this article were performed in parallel with the study by Alawneh et al. [15] using the same protocols with the same users during the same time period. In addition to the performance characterization and comparison, we also conducted preclinical experiments to demonstrate the system's safety and feasibility in vivo using a porcine model.

A. CathPilot Overview

The CathPilot can be used with or in place of a conventional catheter. It utilizes an expandable cable-driven parallel mechanism (X-CADPAM) designed to mitigate the impact of the anatomy (i.e., vessel tortuosity) on steerability. It can be advanced, with the frame collapsed, through a delivery sheath to the target location (e.g., in front of the CTO lesion cap). Once at the target site, the user retracts the delivery sheath to deploy the self-expanding frame of the X-CADPAM. The frame expands up to its designed maximum achievable size or the size permitted by the constraining surrounding anatomy. It provides four anchor points for the four cables that are attached to the catheter tip. Manipulating these cables allows for accurate positioning of the catheter with respect to the frame, and the anatomy to which it is anchored (Fig. 1(c), and (d)). As this is a mechanically over-constrained system, fine position control is achieved regardless of path tortuosity. Due to the redirection of the force around the frame, the movement will be consistent and localized; the effects of external forces that act along the
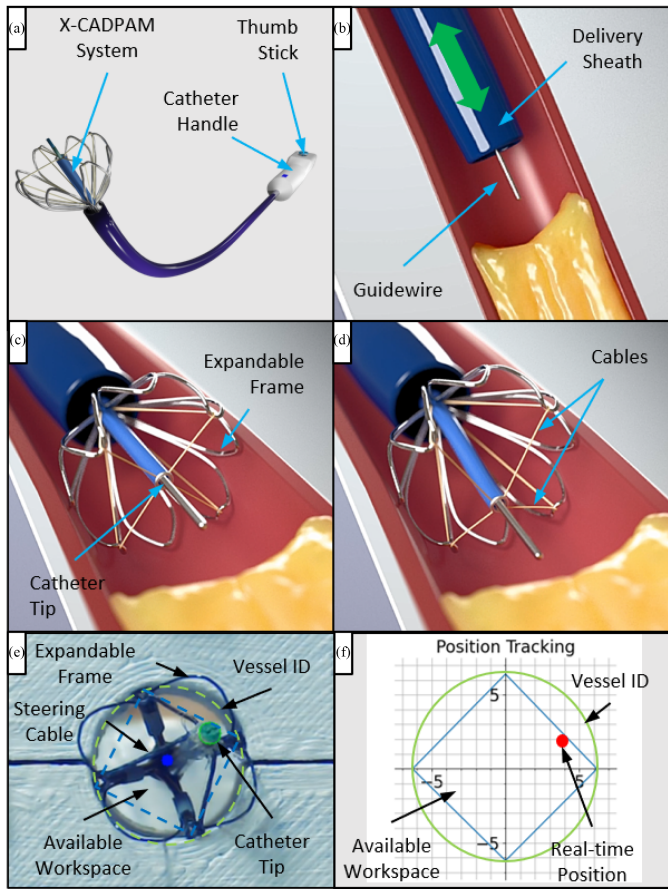
Fig. 1.　(a) CathPilot system. (b) Advancing the CathPilot to the target CTO under the delivery sheath. (c) Fully expanded frame anchoring to the vessel to provide localized steering by redirecting the forces of the cables thereby eliminating the effect of anatomy (i.e., tortuosity) on steering performance. (d) Steering of catheter tip using the four steering cables. (e) CathPilot schematic showing the size of the workspace and the vessel diameter. (f) Graphical user interface indicating real-time position estimation of the CathPilot relative to its available workspace and the vessel diameter.

Fig. 2.　Experimental layout within the catheterization lab showing the CathPilot and its key components, the phantom, and lesion fixtures.

catheter shaft (i.e., tortuosity and bending due to the anatomical constraints) will be mitigated.

The workspace of the catheter is a 2D surface which can be approximated by a plane. The cables run along the length of the catheter and are coupled to a thumbstick in the device handle (Fig. 1(a)). The device is designed such that the motion of the thumbstick on a 2D surface directly maps to the motion of the catheter. Encoders in the handle measure the cable displacements which are then used to estimate the device position in real-time and to visualize it for the user on graphical user interface (GUI) (Fig. 1(f)). With the fluoroscopy system aligned such that the x-ray images are orthogonal to the workspace of the CathPilot plane, the GUI and the x-ray fluoroscopy images together provide 3D feedback for the user to guide the procedure. A beneficial feature of the GUI is that it allows the user to record previously unsuccessful crossing locations (i.e., impenetrable locations in the CTO lesion cap) to allow a systematic approach of finding the optimal path instead of a randomized "poke and pray" approach. The combination of the improved steering and position feedback directly addresses the two key challenges to
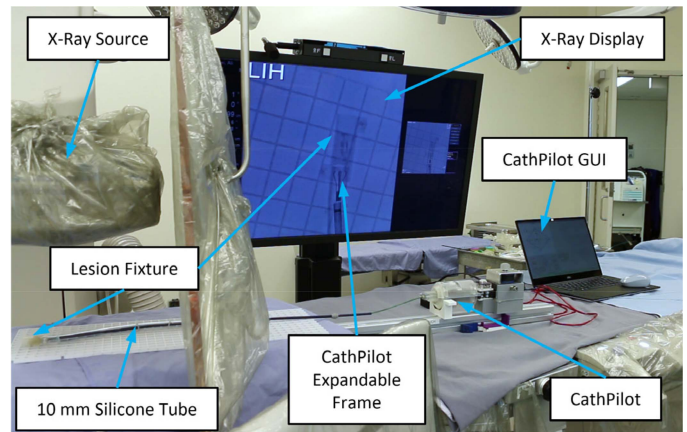
peripheral vascular interventions. A thorough description of the CathPilot system design and features is presented in [21].

In a typical peripheral vascular procedure, the interventionalist advances a guidewire and catheter to the location of the occlusion or stenosis. In the case where the lesion is difficult to cross, the user can swap out the conventional catheter (either a N-SC or a SC) and advance the CathPilot to the lesion for improved catheter steering and visualization. The user uses a delivery sheath to track the CathPilot to the target location; this collapses the expandable frame to allow advancing through the vasculature. Once at the target site, the user retracts the sheath and deploys the self-expandable frame along with the automatically tensioned steering cables. The expandable frame expands up to its designed size or a size constrained by the anatomy. At this point, the user has access to the fine control and visualization afforded by the X-CADPAM system. The user can then systematically try different positions within the CathPilot's workspace to find the optimal path for crossing. An added benefit of the system is that the rigidity of the expandable frame and how it anchors against the vessel wall allows greater force delivery through a guidewire before buckling, which also may improve the success of these procedures [21].

B. Phantom Design

For evaluating the CathPilot, we used the same phantom that replicated the tortuosity of the superficial femoral artery (SFA) as described in [15]. The phantom consists of a 30 cm long silicone tube with an inner diameter (ID) of 10 mm with a prescribed tortuous path; it contains a gradual "s-bend" that has an amplitude of approximately 5 cm. The phantom terminates in a 3D-printed lesion fixture (Formlabs Clear Resin, Formlabs Somerville, MA, USA) that holds the different lesions for the various experiments (Fig. 2). As described in [15], the lesions were either 3D-printed or were CTO tissue samples obtained from amputated limbs of PAD patients who had failed revascularization attempts. The use of actual CTO samples was critical, as, to the best of our knowledge, there is no good model for peripheral CTOs in animals; only human CTOs represent the key challenges for devices in peripheral endovascular interventions.
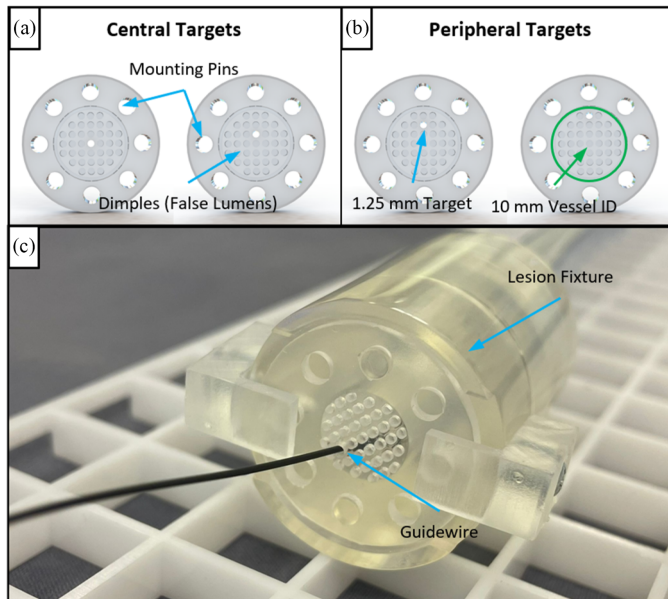
Fig. 3. (a) Central target lesions with 1.25 mm targets at the centre and 1.4 mm from the centre with dimples designed to catch and prevent the guidewire from accidentally accessing the target. (b) Peripheral target lesions with 1.25 mm targets 2.8 mm and 4.2 mm from the centre. (c) Target lesion within the fixture.

C. Experiment Overview

Peripheral vascular interventions require pushing a guidewire through the plaque. Thus, users must access a penetrable location within the lesion cap over the length of an occlusion and apply sufficient force with the guidewire to penetrate and then cross the entire plaque. The following described experiments isolate key aspects of this task.

Experiments 1 to 3 assess the performance of the CathPilot in terms of reaching targets within an arterial phantom model, reachable workspace, and deliverable forces. Experiment 4 evaluates the ability of the CathPilot to cross long CTO samples within an arterial phantom and compares it to conventional devices. Finally, Experiment 5 assesses the CathPilot safety and feasibility in vivo.

1) Experiment 1. Crossing Simulated Plaques: To demonstrate the challenge of navigating a catheter, we used four 3D-printed discs (lesions). Each has a single 1.25 mm target hole at a different position relative to the vessel's center (0 mm, 1.4 mm, 2.8 mm, and 4.2 mm, Fig. 3). We blinded the four users, the same users from [15] (two novice users, one intermediate user with 10 years of catheter design experience, and one expert interventionalist with 15 years of experience) to the location and orientation of the target. This resulted in a total of 16 datapoints (four users and four lesions) using the CathPilot. We gave them 10 minutes under x-ray fluoroscopy to navigate the guidewire with the assistance of the CathPilot and its GUI. The GUI allowed users to see the instantaneous position of the catheter tip (orthogonal to the x-ray plane) and record any locations of failed crossing attempts to avoid unnecessary reattempts at the same site. As previously mentioned, the same task was performed with conventional catheters and reported in
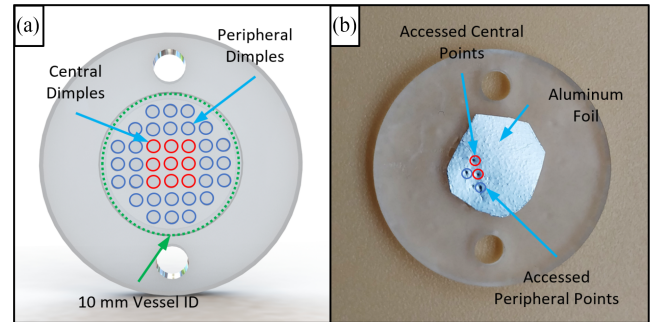

Fig. 4. (a) Backing plate with dimples designed to leave an imprint on the aluminum foil to track the workspace and show the central and peripheral points. (b) Example of accessible workspace with centrally and peripherally accessed positions shown.

[15]. We recorded success rates, procedure times, and radiation exposure.

We compared the success rates of the CathPilot to those for the N-SC and the SC, with a Chi-Squared test using a significance of $\alpha = 0.05$ followed by post-hoc tests to determine any difference between the CathPilot and either the N-SC or the SC. Next, we compared the total procedure times with a one-way analysis of variance (ANOVA, $\alpha = 0.05$) to identify any statistical differences. We then followed with Tukey's multiple comparisons to determine any differences between each device. Finally, we compared the radiation dosage using the same statistical approach.

To understand the relationship between the target location and the success rate of the CathPilot, we grouped the attempts in accessing the central targets (0 mm and 1.4 mm), and the attempts in accessing the peripheral targets (2.8 mm and 4.2 mm). We compared the success rates, procedure times, and radiation dosages for all three devices using the same statistical approach as previously mentioned.

2) Experiment 2. Workspace Evaluation: A good catheter for peripheral revascularization should allow the user to effectively access the entire cross-section of the artery to find penetrable sections of the plaque cap.

To evaluate the reachable workspace of the CathPilot, like our other study [15] we attached a piece of aluminum foil to the surface of the dimpled plate containing 37 dimples (Fig. 4). The foil and dimples permit tracing the reached workspace by the guidewire. We provided 5 minutes for the users (n = 4) to trace as much of the vessel's cross-sectional area as possible using the guidewire and the CathPilot with its corresponding GUI and with x-ray guidance. We counted the total number of dimple traces on the aluminum foil out of the maximum 37 locations to calculate the percentage of covered area. We then compared the CathPilot's area coverage with those of conventional catheters as previously reported in [15].

We divided the cross-section into two different segments – the central region (within 2.5 mm from the centre, Fig. 4) and the peripheral region (beyond 2.5 mm from the centre, Fig. 4). We compared the area coverage of all three catheters (one-way ANOVA, $\alpha = 0.05$): the total area coverage, the central area coverage, and the peripheral area coverage. We followed this
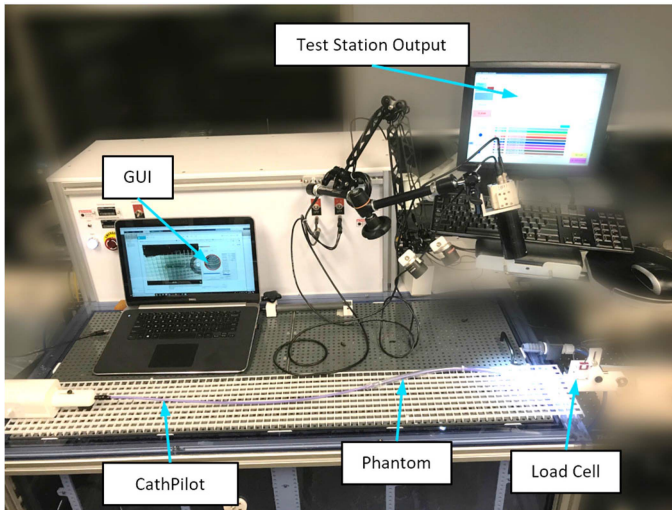
Fig. 5. Experimental layout showing the position of the phantom, the force gauge, and the CathPilot.
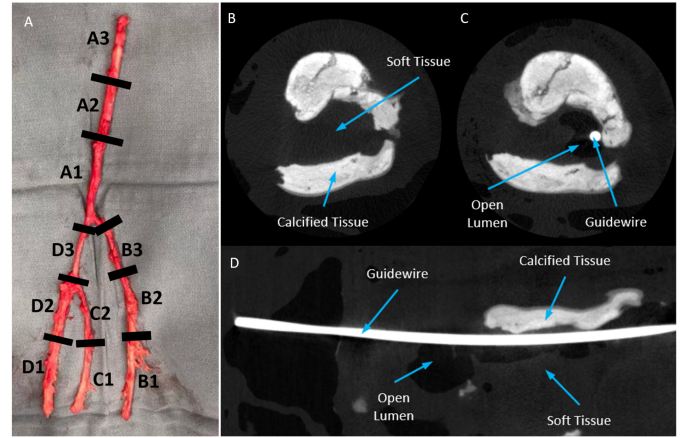

Fig. 6. (a) shows the harvested peripheral artery used as fresh samples and how it was segmented; (b) Pre-procedural axial CT image of the lesion showing soft and calcified tissue; (c) Post-procedural axial CT image showing guidewire location relative to the open lumen; (d) Post-procedural coronal CT image showing complete guidewire penetration of lesion.

with Tukey's multiple comparisons to compare the N-SC and the SC to the CathPilot.

3) Experiment 3. Force Delivery: We know that plaques are heterogeneous, and the various components require different levels of force for penetration of the guidewire [9], [22]. Therefore, it is essential to quantify the support a catheter provides for guidewire pushability. With the phantom in a catheter test station (IDTE 200; Machine Solutions inc., Flagstaff, AZ, USA) and the lesion fixture in line with a 100 g load cell (accuracy ± 3 g, Machine Solutions Inc., USA), users had one minute to repeatedly hit the force sensor using either a 0.035" J-tipped guidewire or a straight guidewire supported by the CathPilot (Fig. 5). We isolated the peak forces ($n \approx 100$ for the J-tipped guidewire and CathPilot and $n \approx 100$ for the straight guidewire and CathPilot), and we pooled the previous data from the N-SC, the SC, and the CathPilot to determine any statistically significant differences (one-way ANOVA, $\alpha = 0.05$), followed by Tukey's multiple comparisons for each individual group.

4) Experiment 4. Ex Vivo Crossing of CTO Samples: We assessed the CathPilot's performance in the crossing of both fixed and fresh CTO samples obtained from donated amputated limbs of CLI patients with failed endovascular attempts. Obtaining these samples and the corresponding experiments were approved by the Sunnybrook Health Research Centre Research Ethics Board under project No. 2249. Including both fresh and fixed samples allowed to assess and compare for potential differences in performance to facilitate potential future experiments with fixed samples [23], [24], [25].

For the experiments with fixed samples, we obtained the CTO samples from the popliteal and tibial arteries from a 65-year-old male amputee with chronic limb ischemia (CLI, i.e., late-stage PAD). The samples were fixed in a 10% buffered formalin solution (Sigma-Aldrich, St. Louis, MS, USA) at 4°C. To establish a pre-procedural baseline, we imaged the ex vivo vessels under μCT (Scanco μCT 100; Scanco Medical, Brüttisellen, Switzerland) with the following parameters: $50 \times 50 \times 50 \, \mu m^3$, 55 kVp, 200 μA, 11 W.

We cut the lesions into segments of 21.9 ± 7.0 mm. We chose this length so that we would have a minimum of 6 samples to permit multiple attempts and permit statistical analysis of the results. The samples had an average ID of 3.1 ± 0.8 mm. They were secured in a lesion holder 70 mm in length. Like the previous study [15] and experiment 1, each user had 10 minutes to cross each lesion using the CathPilot, defining success as a transluminal crossing (Fig. 6). To verify a successful transluminal crossing, we cut the guidewire while still in the fixture, and we imaged the assembly with μCT. As the users were free to choose from any of the following guidewires: J and straight tip 0.035" Glidewire, as well the following 0.014" guidewires: the Hi-Torque Winn[TM] 40 (Abbott Laboratories, Chicago, IL, USA), the Hi-Torque Winn[TM] 80 (Abbott Laboratories, USA), the Hi-Torque Winn[TM] 200T (Abbott Laboratories, USA), or the Hi-Torque Command[TM] ES (Abbott Laboratories, USA). Users were also able to use a 2.3Fr microcatheter (CXI, Cook Medical, USA) which allowed them to extend the support of the CathPilot from the location of anchor to the lesion while using 0.014" guidewires. Crossing of the same lesions were then attempted immediately after with the conventional N-SC (and reported in [15]) with the same options for guidewires and microcatheters, and results were compared.

Following the completion of the crossing experiments, each lesion was subjected to a subsequent μCT scan, employing the parameters previously outlined. This allowed for a comprehensive assessment of the guidewire crossing paths, and facilitated the determination of whether subintimal or intraluminal crossings were achieved. Additionally, the presence of any vessel wall perforations was evaluated. Notably, during the experiments, perforations could also be visually detected, as the lesion holders were made of semi-transparent material.

We recorded success rates, total procedure times, and radiation dosages and compared them to the non-steerable catheter (steerable catheters are not typically used during peripheral

interventions), using Fisher's exact test for the success rate and two-tailed t-tests for the times and radiation dosages, all with a significance of $\alpha = 0.05$.

We performed the same experiments on fresh tissue samples consisting of popliteal and tibial arteries from a 63-year-old female with CLI after amputation stored at 4°C in 0.9% saline. As a larger sized sample was available (Fig. 6(a)), we were able to cut it to longer lengths of 47.6 ± 3.6 mm segments with the vessels having an average ID of 3.3 ± 1.1 mm. We stored the lesions at -18°C, thawing them to ambient temperatures prior to each procedure. We performed these experiments within 48 hours of amputation. Overall, we were able to acquire 6 datapoints for the fixed tissue and 18 datapoints for the fresh tissue.

5) Experiment 5. In Vivo Safety and Feasibility Study:
The goal of this experiment was to test the following: the feasibility of using the device in a conventional interventional procedure and its reliable functionality in vivo, potential damage to the arterial wall, and the device's thrombogenicity. This study was approved by Sunnybrook Health Research Centre under Animal Use Protocol No. 235.

For our experiments, a male pig (56.6 kg) was used. Heparin anticoagulant (100IU/kg direct injection and 2000IU in IV) was administered. Procedures were performed by a vascular interventionalist with more than 15 years of experience. To create blood flow dynamics like those in an arterial occlusion, a balloon catheter (7mm OD, Abbott Armada 35 PTA) was advanced from the carotid artery and deployed midway through the aorta. Using a right-side femoral artery access, a non-steerable 12 Fr sheath (Cook Medical G56279) was advanced with standard methods and positioned inferior to the balloon. The CathPilot was advanced through this delivery sheath and deployed at the target site inferior to the renal arteries (Fig. 2). With the frame of the CathPilot anchored onto the anatomy, the internal catheter containing a J-tipped 0.35" guidewire (Glidewire, Terumois, Japan) was steered and manipulated for 15 minutes with its motion confirmed via fluoroscopy to verify catheter functionality. Every 5 minutes the system was flushed with saline (∼10mL each time). We used 2 CathPilot systems for two datapoints – one datapoint for catheter manipulation in the presence of normal blood flow (without the occluding balloon) and one datapoint under occult conditions (with the occluding balloon).

Immediately after each procedure, the CathPilot was withdrawn and inspected visually for signs of coagulation. The pig was euthanized, and the artery was excised and cut open to assess for any visual signs of damage or trauma to the endothelial layer at the site of CathPilot deployment.

III. RESULTS

A. Experiment 1: Crossing Simulated Plaques

Table I summarizes the results for experiment 1: the success rates, the procedure times, and the radiation dosages. For all targets (i.e., shown in Fig. 3), we observed a statistically significant difference between the success rates (p = 0.0002, chi-Squared test), the procedure times (p<0.0001, one-way ANOVA), and the radiation dosages (p<0.0001, one-way ANOVA). The post-hoc

TABLE I
SUMMARY OF SUCCESS RATES, PROCEDURE TIMES, AND RADIATION DOSAGES

	None-Steerable Catheter (N-SC)	Steerable Catheter (SC)	CathPilot
Success Rates			
Total	31% (5/16)	69% (11/16)	**100% (16/16)**
Central	12.5% (1/8)	75% (6/8)	**100% (8/8)**
Peripheral	50% (4/8)	62.5% (5/8)	**100% (8/8)**
Procedure Times [avg. ± SD] [s]			
Total	436±252 (n=16)	299±236 (n=16)	**74.6±52.1 (n=16)**
Central	528±203 (n=8)	225±237 (n=8)	**80.6±56.2 (n=8)**
Peripheral	345±276 (n=8)	373±226 (n=8)	**68.6±50.8 (n=8)**
Radiation Dosage [avg. ± SD] [mGy]			
Total	0.90±0.50 (n=16)	0.67±0.13 (n=16)	**0.13±0.11 (n=16)**
Central	1.03±0.41 (n=8)	0.48±0.45 (n=8)	**0.15±0.13 (n=8)**
Peripheral	0.78±0.58 (n=8)	0.86±0.53 (n=8)	**0.10±0.07 (n=8)**

tests reveal further differences between statistical differences between the success rates for the CathPilot and the N-SC, the CathPilot and the SC, but not the N-SC and the SC (p<0.0001, p = 0.043, and p = 0.076, respectively; Fisher's exact test). We found the same trends for the procedure times (p<0.0001, p = 0.0081, and p = 0.14, for the CathPilot vs. the N-SC, the CathPilot vs. the SC, and the N-SC vs the SC, respectively) and radiation dosages (p<0.0001, p = 0.0017, and p = 0.28, respectively).

To further analyze the impact of the target position on the crossing success rate, we divided the targets into central targets (0 mm and 1.4 mm from the centre) and peripheral targets (2.8 mm and 4.2 mm from the centre). We found statistical differences between the success rates for the central targets (p = 0.001, Chi-Squared test); further post-hoc tests showed differences between the CathPilot and the N-SC (p = 0.0014), the N-SC and the SC (p = 0.041), but no differences between the CathPilot and the SC (p = 0.47). For the peripheral targets, we found no statistical differences between the catheters (p = 0.073, Chi-Squared test).

Next, we analyzed the impact of the target position on the procedure times. We found a statistical difference for the procedure times for the central targets (p = 0.0003, one-way ANOVA) with post-hoc testing revealing differences between the N-SC and the SC (p = 0.0089), the CathPilot and the N-SC (p = 0.0002), but no differences between the CathPilot and the SC (p = 0.28). Unlike the success rates, we found statistical differences for the peripheral procedure times (p = 0.014, one-way ANOVA) with differences between the CathPilot and the N-SC (p = 0.037), the CathPilot and the SC (p = 0.021), but no differences between the N-SC and the SC (p = 0.96).

Finally, we analyzed the impact of the target position on the radiation dosages. These results followed the same trend as the procedure times. We found a statistical difference between the
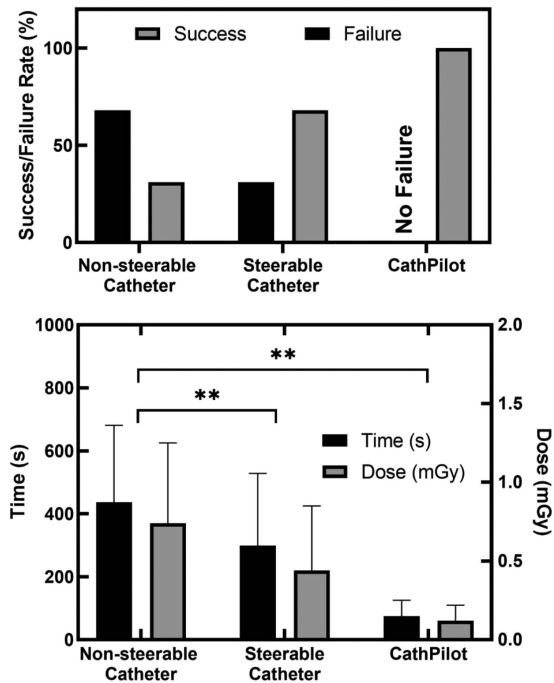
Fig. 7. (a) Success and failures for each catheter within the phantom model with 3D printed lesions. (b) Crossing times and radiation dosages for the phantom experiments with 3D printed lesions (ANOVA, p<0.05).
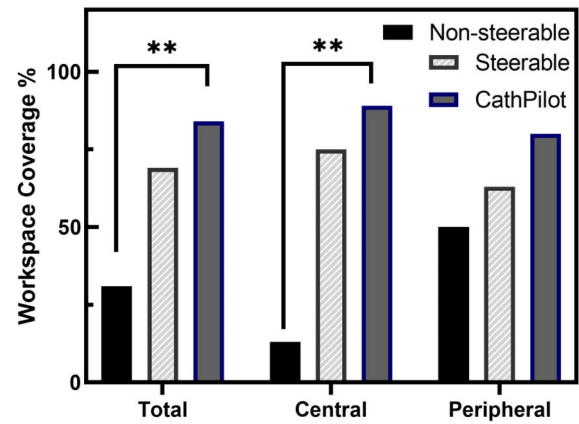

Fig. 8. Workspace coverage for the total possible area, central target area, peripheral target area, for the three different catheters. Overall, the CathPilot significantly outperforms the other catheters in terms of reachable workspace and surface coverage (ANOVA, p<0.05).

catheters for the central targets (p = 0.0003, one-way ANOVA) with differences between the N-SC and the SC (p = 0.016), the CathPilot and the N-SC (p = 0.0002), but no differences between the CathPilot and the SC (p = 0.19). for the peripheral targets, we found a statistical difference between the catheters (p = 0.0052, one-way ANOVA) with differences between the CathPilot and the N-SC (p = 0.019), the CathPilot and the SC (p = 0.0077), but no differences between the N-SC and the SC (p = 0.92). Fig. 7 shows a complete graphical representation of the success rates, the procedure times, and the radiation dosages while indicating the groups with observed statistical differences. One key thing of note: although the CathPilot did not statistically outperform the SC in terms of the segmented success rates, the fact that the CathPilot showed a 100% success rate is important. We found the same trend with the shorter procedure times and the lesser radiation dosage. These factors have the potential to improve these procedures for interventionalists and patients.

The following section shows the results of our workspace evaluation, which can explain the differences in the metrics for experiment 1 in all targets, the central targets, and the peripheral targets.

B. Experiment 2: Workspace Evaluation

When comparing the reachable workspace within the full area, we found a significant difference (one-way ANOVA, p = 0.0025, Fig. 8) between the N-SC ($35.8 \pm 18.6\%$, n = 4), the SC ($63.5 \pm 12.0\%$, n = 4), and the CathPilot ($81.8 \pm 4.6\%$, n = 4). Further post-hoc analysis using Tukey's multiple comparisons revealed significant differences between the N-SC and the CathPilot (p = 0.002). However, we did not find any significant differences

between the SC and the CathPilot (p = 0.17). these results follow the trend indicated by experiment 1, where the CathPilot statistically outperformed the N-SC for all targets.

When we analyzed the central workspace, we found a statistical difference between all of the catheters (p<<0.001, one-way ANOVA; p<0.03, Tukey' multiple comparisons), where the N-SC, the SC, and the CathPilot covered $2.8 \pm 5.6\%$ (n = 4), $63.9 \pm 27.8\%$ (n = 4), and 100% (n = 4) of the central area, respectively. These results also follow the trend indicated by experiment 1, with one exception. The CathPilot statistically outperformed the SC for the central workspace. This suggests that, in lesions with centrally located channels, the CathPilot may provide easier access. In addition, the lack of significance between the CathPilot and the SC in experiment 1 may have been a result of a small sample size.

Finally, when we analyzed the peripheral workspace, we found no statistical difference between the catheters (one-way ANOVA, p = 0.097, Fig. 8), with the N-SC, the SC, and the CathPilot covering $46.4 \pm 23.9\%$ (n = 4), $63.4 \pm 15.8\%$ (n = 4), and $75.9 \pm 6.1\%$ (n = 4) of the peripheral area, respectively. This, again, reflects the results of experiment 1, where there were no significant differences between each catheter in accessing peripheral targets.

Finally, when we analyzed the peripheral workspace, we found no statistical difference between the catheters (one-way ANOVA, p = 0.097, Fig. 8), with the N-SC, the SC, and the CathPilot covering $46.4 \pm 23.9\%$ (n = 4), $63.4 \pm 15.8\%$ (n = 4), and $75.9 \pm 6.1\%$ (n = 4) of the peripheral area, respectively. This, again, reflects the results of experiment 1, where there were no significant differences between each catheter in accessing peripheral targets.

C. Experiment 3: Force Delivery

In addition to the workspace, another key aspect of peripheral vascular interventions is force-delivery. In our experiment, we measured the force exerted by a guidewire when supported by the CathPilot and compared these values to those of the N-SC and the SC, as reported by the previous study [15]. We found
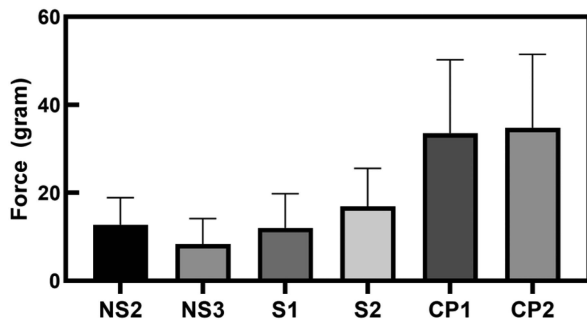
Fig. 9. Peak force delivery for each guidewire and catheter combination. NS1: a straight guidewire with a bent tip non-steerable microcatheter; NS2: a J-shaped guidewire with a bent tip non-steerable microcatheter; NS3: a straight guidewire with a straight non-steerable microcatheter; S1: a straight guidewire with a steerable catheter; S2: a J-shaped guidewire with a steerable catheter; CP1: a straight guidewire with the CathPilot; and CP2: a J-shaped guidewire with the CathPilot.
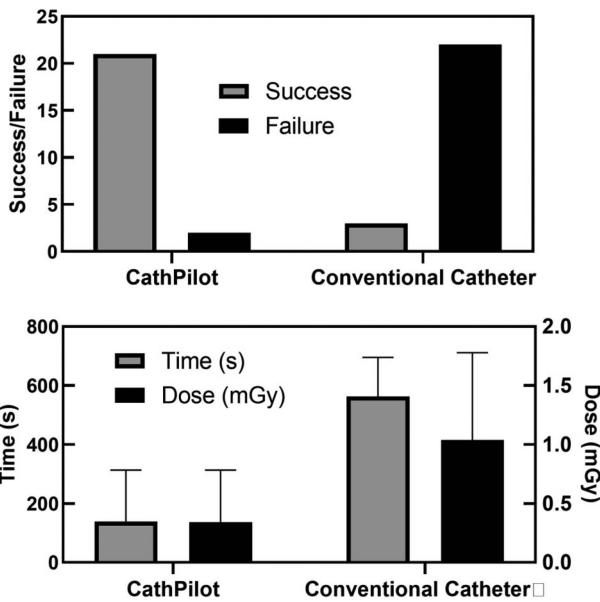

Fig. 10. (a) Overall success rates of the CathPilot vs. the Conventional non-steerable catheter in crossing CTO samples (fresh and fixed) harvested from amputated limbs of CLI patients with past failed revascularization attempts. (b) Combined procedure times and administered dose (i.e., proportional to fluoroscopy time) for the corresponding procedures. The CathPilot significantly outperforms the conventional non-steerable catheter in both metrics (p<<0.05, ANOVA).

TABLE II
SUMMARY OF RESULTS OF EX VIVO CROSSING OF CTO SAMPLES

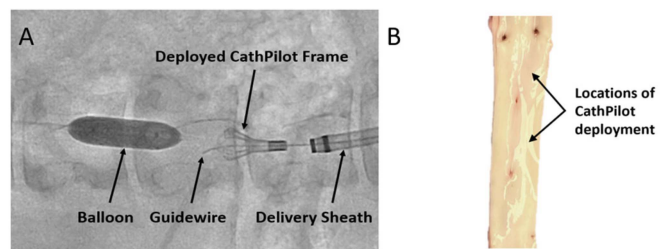|	Success Rate		
	None-Steerable Catheter	CathPilot	P-Value
Fresh	9.5% (2/21)	83.3% (15/18)	0.0001*
Fixed	0% (0/6)	100% (6/6)	0.002*
	Procedure Times [avg. ± SD] [s]		
Fresh	556±143 (n=21)	152±212 (n=18)	~0.0*
Fixed	600±0 (n=6)	175±147 (n=6)	0.0009*
	Radiation Dosage [avg. ± SD] [mGy]		
Fresh	0.48±0.54 (n=21)	0.17±0.26 (n=18)	0.02*
Fixed	1.42±0.73 (n=6)	0.71±0.58 (n=6)	0.09

Fig. 11. (a) shows X-ray images of the CathPilot as deployed within the subject's aorta in front of the balloon. (b) shows the excised and opened aorta and identifies the locations of CathPilot deployment without any indications of damage or trauma to the vessel wall.

For fresh CTO samples, we found similar results with the CathPilot outperforming the N-SC in crossing success (p = 0.0001, Fisher's exact test, Fig. 10(a)), in procedure times (p~0.0, two-tailed t-test, Fig. 10(b)), and in radiation dosage (p = 0.02, two-tailed t-test, Fig. 10(b)). The results are summarized in Table II.

With regards to perforation, the CathPilot method led to only perforation of the vessel wall, while the conventional methods perforated the vessel wall on nine occasions.

E. Experiment 5: In Vivo Safety and Feasibility Study

We performed two different tests with the CathPilot. The first test was in a high blood flow environment without the balloon replicating the occlusion. The experienced interventionalist introduced and retracted the CathPilot and manipulated the cables to steer the catheter. During this 15-minute procedure, we confirmed that the CathPilot was fully functional throughout the experiment; the interventionalist successfully steered the device within the entire workspace, as validated by fluoroscopy (Fig. 11(a)), without any mechanical issues. The second test was in an occlusive environment where an upstream balloon restricted blood flow, thereby replicating the environment around a CTO. Again, during the entire 15-minute procedure, we confirmed full functionality and there were no signs of coagulation on the device despite the stagnant blood surrounding the device. Upon excision and visual inspection of the aorta, we found no visible signs of damage or trauma to the endothelium nor

a statistical difference between the seven different guidewire and catheter combinations (p~0.0, one-way ANOVA, n≈100 per group, Fig. 9). When we grouped the data for each catheter, there was a statistically significant difference between the N-SC, the SC, and the CathPilot, achieving 10.2 ± 8.1 g, 14.2 ± 8.4 g, and 40.4 ± 14.2 g, respectively (p~0.01, one-way ANOVA).

D. Experiment 4: Ex Vivo Crossing of CTO Samples

For fixed CTO samples, the CathPilot achieved a significantly greater success rate than the N-SC (p = 0.002, Fisher's exact test, Fig. 10A) with a significantly faster procedure time and reduced dosage (p = 0.0009, two-tailed t-test, Fig. 10(b)).

any deeper damage to the vessel at the positions of CathPilot deployment (Fig. 11(b)).

IV. DISCUSSION

This study quantifies the performance of a novel steerable catheter, the CathPilot, and compares it to conventional non-steerable and steerable catheters in the context of minimally invasive peripheral vascular interventions. With lesion crossing being the most crucial step in endovascular revascularization procedures, we demonstrated the effectiveness of the CathPilot in crossing such lesions (both 3D printed and CTO samples from patients). We also quantified the device's reachable workspace (i.e., steerability) and the force it allows to be delivered by the guidewire (i.e., pushability). More importantly, we also demonstrated the device's safety and feasibility in vivo.

Results indicate the CathPilot statistically outperformed the conventional catheters in most categories – the reachable workspace, the higher delivery forces, and the success rates in crossing our 3D printed lesions. Even in the cases where no statistical significance was found compared with the SC, being successful in 100% of cases while taking less time may mean improvements in the cath-lab. More importantly, the CathPilot significantly outperformed the conventional catheters in crossing actual occlusion samples. The CathPilot outperformed conventional catheters with regard to fluoroscopy time, procedure time, and importantly perforation rate. The preclinical studies also showed that there were no visible signs of damage to the vessel wall, and there were no signs of coagulation on the device. These results demonstrate the potential of the CathPilot concept to reduce failure rates and complication rates [26], [27], [28], [29], [30], while reducing radiation exposure of all involved parties[31].

It is important to highlight that applying force through a guidewire is vital to crossing the plaque. A previous study showed that even the "soft" lesions with thrombotic and collagenous plaques required, on average, 0.43 N or 44 g to cross [9]. The conventional devices were only able to provide, on average, a quarter of that load. On the other hand, in experiment 3, the CathPilot could support significantly greater forces before buckling the guidewire. However, greater force output means a greater risk of vessel perforation. We believe that the CathPilot mitigates this risk—as demonstrated in the results—by providing the position control needed to steer the guidewire away from the vessel wall. This positioning control may potentially also help reduce the risks of other specialized devices that have the potential of causing further damage to the vessel (e.g., atherectomy devices and RF-ablation guidewires) [10], [22]. As part of future studies, we plan to test the CathPilot with such devices within a full amputated leg model to assess the system's potential added value.

There are a few limitations to this study. Firstly, steerable catheters were not used in crossing of CTO samples due to the limited number of samples available for the experiments. This was justified as steerable catheters are seldom used during peripheral endovascular interventions. Another limitation of the study was that the CTOs used belonged to CLI patients with past failed revascularization attempts and most likely represented the worst-case scenario for all systems. However, despite these circumstances, the CathPilot successfully crossed most of the lesions and outperformed conventional non-steerable catheters. Another limitation of the current study is that it only tested the CathPilot system at a 12Fr size and not at the preferred size of 6-8Fr, which is currently under development. However, these initial results demonstrate the added value of the Cath-Pilot system concept and the potential added value it provides by enhancing steerability, pushability and 3D visualization. In addition, we acknowledge that our sample size was limited; however, the CathPilot was still able to statistically outperform conventional catheters in most cases – even in the case where no statistical difference was found, the improvement offered by a 100% success rate (for crossing 3D printed lesions) shows the potential of the CathPilot. Finally, we note the single porcine model as a limitation in our in vivo experiment; although the results are hopeful, we will need more samples to understand the safety of the CathPilot. We hope to address these limitations in future steps of our research.

The following steps for this research include evaluating the 7Fr version of the CathPilot within fresh and full amputated limbs of CLI patients. We believe that a in situ full limb model will be the best setup for device testing before the initiation of our clinical studies.

V. CONCLUSION

In this study, we aimed to meticulously quantify the performance of the CathPilot system and compare its performance to traditional non-steerable and steerable catheters, focusing on critical metrics for peripheral vascular interventions. Our findings show that the CathPilot system outperforms conventional devices in terms of reachable workspace, guidewire-delivered forces, and successful crossing of arterial occlusions. Furthermore, this study provides evidence supporting the safety and feasibility of utilizing the CathPilot system in vivo, showcasing its potential to enhance clinical outcomes in peripheral vascular interventions.

REFERENCES

[1] S. S. Virani et al., "Heart disease and stroke statistics—2020 update: A report from the American Heart Association," *Circulation*, vol. 141, no. 9, pp. E139–E596, Mar. 2020, doi: 10.1161/CIR.0000000000000757.

[2] M. H. Criqui and V. Aboyans, "Epidemiology of peripheral artery disease," *Circ. Res.*, vol. 116, no. 9, pp. 1509–1526, Apr. 2015, doi: 10.1161/CIR-CRESAHA.116.303849.

[3] M. S. Conte, "Critical appraisal of surgical revascularization for critical limb ischemia," *J. Vasc. Surg.*, vol. 57, pp. 8S–13S, 2013. doi: 10.1016/j.jvs.2012.05.114.

[4] B. A. Golomb, T. T. Dang, and M. H. Criqui, "Peripheral arterial disease: Morbidity and mortality implications," *Circulation*, vol. 114, no. 7, pp. 688–699, Aug. 2006. doi: 10.1161/CIRCULATIONAHA.105.593442.

[5] F. G. R. Fowkes et al., "Peripheral artery disease: Epidemiology and global perspectives," *Nature Rev. Cardiol.*, vol. 14, no. 3, pp. 156–170, Nov. 2016, doi: 10.1038/nrcardio.2016.179.

[6] D. J. Adam et al., "Bypass versus angioplasty in severe ischaemia of the leg (BASIL): Multicentre, randomised controlled trial," *Lancet*, vol. 366, no. 9501, pp. 1925–1934, Dec. 2005, doi: 10.1016/S0140-6736(05)67704-5.

[7] O. Iida et al., "Long-term results of direct and indirect endovascular revascularization based on the angiosome concept in patients with critical limb ischemia presenting with isolated below-the-knee lesions," *J. Vasc. Surg.*, vol. 55, no. 2, pp. 363–370.e5, Feb. 2012, doi: 10.1016/j.jvs.2011.08.014.

[8] M. B. Malas et al., "Comparison of surgical bypass with angioplasty and stenting of superficial femoral artery disease," *J. Vasc. Surg.*, vol. 59, pp. 129–135, 2014, doi: 10.1016/j.jvs.2013.05.100.

[9] T. Roy et al., "Puncturing plaques: Relating MRI characteristics of peripheral artery lesions to guidewire puncture forces," *J. Endovascular Ther.*, vol. 24, no. 1, pp. 35–46, 2017, doi: 10.1177/1526602816671135.

[10] T. Roy, A. D. Dueck, and G. A. Wright, "Peripheral endovascular interventions in the era of precision medicine: Tying wire, drug, and device selection to plaque morphology," *J. Endovascular Ther.*, vol. 23, no. 5, pp. 751–761, Oct. 2016, doi: 10.1177/1526602816653221.

[11] T. L. Roy et al., "Magnetic resonance imaging characteristics of lesions relate to the difficulty of peripheral arterial endovascular procedures," *J. Vasc. Surg.*, vol. 67, no. 6, pp. 1844–1854.e2, Jun. 2018, doi: 10.1016/j.jvs.2017.09.034.

[12] R. B. Allan and C. L. Delaney, "Identification of micro-channels within chronic total occlusions using contrast-enhanced ultrasound," *J. Vasc. Surg.*, vol. 74, no. 2, pp. 606–614.e1, Aug. 2021, doi: 10.1016/J.JVS.2020.12.108.

[13] A. Ali et al., "Catheter steering in interventional cardiology: Mechanical analysis and novel solution," *Proc. Inst. Mech. Engineers, Part H: J. Eng. Med.*, vol. 233, no. 12, pp. 1207–1218, Dec. 2019, doi: 10.1177/0954411919877709.

[14] A. Ali, D. H. Plettenburg, and P. Breedveld, "Steerable catheters in cardiology: Classifying steerability and assessing future challenges," *IEEE Trans. Biomed. Eng.*, vol. 63, no. 4, pp. 679–693, Apr. 2016, doi: 10.1109/TBME.2016.2525785.

[15] Y. Alawneh et al., "Experimental protocol and phantom design and development for performance characterization of conventional devices for peripheral vascular interventions," *Ann. Biomed. Eng.*, pp. 1–11, Feb. 2023, doi: 10.1007/s10439-023-03160-x.

[16] H. Rafii-Tari, C. J. Payne, and G. Z. Yang, "Current and emerging robot-assisted endovascular catheterization technologies: A review," *Ann. Biomed. Eng.*, vol. 42, no. 4, pp. 697–715, 2014, doi: 10.1007/s10439-013-0946-8.

[17] F. Kiemeneij et al., "Use of the stereotaxis Niobe magnetic navigation system for percutaneous coronary intervention: Results from 350 consecutive patients," *Catheterization Cardiovasc. Interv.*, vol. 71, no. 4, pp. 510–516, Mar. 2008, doi: 10.1002/ccd.21425.

[18] J. Hwang, J. young Kim, and H. Choi, "A review of magnetic actuation systems and magnetically actuated guidewire- and catheter-based micro-robots for vascular interventions," *Intell. Service Robot.*, vol. 13, no. 1, pp. 1–14, Jan. 2020, doi: 10.1007/S11370-020-00311-0.

[19] C. Shi et al., "Shape sensing techniques for continuum robots in minimally invasive surgery: A survey," *IEEE Trans. Biomed. Eng.*, vol. 64, no. 8, pp. 1665–1678, Aug. 2017, doi: 10.1109/TBME.2016.2622361.

[20] A. M. Franz et al., "Electromagnetic tracking in medicine—A review of technology, validation, and applications," *IEEE Trans. Med. Imag.*, vol. 33, no. 8, pp. 1702–1725, 2014, doi: 10.1109/TMI.2014.2321777.

[21] J. J. Zhou et al., "The CathPilot: A novel approach for accurate interventional device steering and tracking," *IEEE/ASME Trans. Mechatron.*, vol. 27, no. 6, pp. 5812–5823, Dec. 2022, doi: 10.1109/TMECH.2022.3188955.

[22] M. A. Tavallaei et al., "Performance assessment of a radiofrequency powered guidewire for crossing peripheral arterial occlusions based on lesion morphology," *Ann. Biomed. Eng.*, vol. 46, no. 7, pp. 940–946, Jul. 2018, doi: 10.1007/s10439-018-2021-y.

[23] H. W. Sung et al., "Mechanical properties of a porcine aortic valve fixed with a naturally occurring crosslinking agent," *Biomaterials*, vol. 20, no. 19, pp. 1759–1772, Oct. 1999, doi: 10.1016/S0142-9612(99)00069-1.

[24] E. W. Flitney et al., "Insights into the mechanical properties of epithelial cells: The effects of shear stress on the assembly and remodeling of keratin intermediate filaments," *FASEB J.*, vol. 23, no. 7, pp. 2110–2119, Jul. 2009, doi: 10.1096/FJ.08-124453.

[25] Y. Ling et al., "Effects of fixation and preservation on tissue elastic properties measured by quantitative optical coherence elastography (OCE)," *J. Biomech.*, vol. 49, no. 7, pp. 1009–1015, May 2016, doi: 10.1016/J.JBIOMECH.2016.02.013.

[26] T. Roy et al., "Burning bridges: Mechanisms and implications of endovascular failure in the treatment of peripheral artery disease," *J. Endovascular Ther.*, vol. 22, no. 6, pp. 874–880, Dec. 2015, doi: 10.1177/1526602815604465.

[27] A. W. Bradbury et al., "Bypass versus Angioplasty in Severe Ischaemia of the Leg (BASIL) trial: Analysis of amputation free and overall survival by treatment received," *J. Vasc. Surg.*, vol. 51, no. 5 SUPPL., pp. 18S–31S, 2010, doi: 10.1016/j.jvs.2010.01.074.

[28] R. Ross, "Atherosclerosis - An inflammatory disease," *New England J. Med.*, vol. 340, no. 2, pp. 115–126, Jan. 1999. doi: 10.1056/NEJM199901143400207.

[29] V. M. Subbotin, "Analysis of arterial intimal hyperplasia: Review and hypothesis," *Theor. Biol. Med. Model.*, vol. 4, 2007, Art. no. 41, doi: 10.1186/1742-4682-4-41.

[30] L. P. Zielinski, M. M. Chowdhury, and P. A. Coughlin, "Patient and institutional costs of failure of angioplasty of the superficial femoral artery," *Ann. Vasc. Surg.*, vol. 72, pp. 218–226, Apr. 2021, doi: 10.1016/j.avsg.2020.08.106.

[31] E. R. Ketteler and K. R. Brown, "Radiation exposure in endovascular procedures," *J. Vasc. Surg.*, vol. 53, pp. 35S–38S, 2011, doi: 10.1016/J.JVS.2010.05.141.